INTERNATIONAL JOURNAL OF MULTIDISCIPLINARY COMPREHENSIVE RESEARCH

# Multi-Sensor Assessment of Mangrove Canopy Dynamics in Can GIO, Vietnam, Using Sentinel-1 and Sentinel-2

**Hoang Thi Thuy [1*], Ngo Thi Minh The [2], Le Thi Lan Thao [3]**
[1-3] Nong Lam University, Ho Chi Minh City, Vietnam

* Corresponding Author: **Hoang Thi Thuy**

## Article Info

**ISSN (online):** 2583-5289
**Volume:** 05
**Issue:** 06
**Received:** 08-09-2026
**Accepted:** 06-10-2026
**Published:** 04-11-2026
**Page No:** 14-23

**Abstract**
Monitoring mangrove ecosystems in tropical estuaries remains challenging because persistent cloud cover, complex forest–water interfaces, and variations in satellite observation coverage can affect the consistency of long-term assessments. Integrating optical and radar observations offers opportunities to characterize mangrove-related variability, although comparisons across years may be influenced by differences in the spatial extent of valid observations. This study examines the spatial and temporal variability of mangrove-related optical and radar indices in Can Gio, Vietnam, from 2021 to 2025, using Sentinel-2 normalized difference vegetation index (NDVI) and normalized difference moisture index (NDMI), together with Sentinel-1 dual-polarization radar vegetation index (RVI). Annual satellite-derived raster products were reanalysed using a consistent spatial framework comprising 818,487 valid pixels at 20-m resolution, covering approximately 32,739.48 ha. The results revealed distinct temporal patterns among the three indices. NDVI and NDMI reached their highest annual means in 2022 (0.8234 and 0.5207, respectively), whereas RVI peaked in 2024 (0.7981) before declining to 0.7854 in 2025. Over the study period, mean NDVI and NDMI increased slightly by 0.00352 and 0.00271, respectively, while RVI decreased by 0.00980. Spatial analysis further revealed heterogeneous patterns of positive and negative changes across the study area, highlighting differences in optical and radar responses. These findings demonstrate the value of integrating complementary satellite observations within a consistent spatial framework for characterizing mangrove-related index variability. The resulting spatial information provides a basis for identifying areas requiring further investigation and supporting mangrove monitoring, while recognizing that satellite-index changes alone cannot establish ecological degradation or its underlying causes.

**DOI:** https://doi.org/10.54660/IJMCR.2026.5.6.14-23

**Keywords:** Can Gio, mangrove, normalized difference moisture index, radar vegetation index, Sentinel-2

## 1. Introduction

Mangrove ecosystems provide shoreline protection, habitat, sediment retention and substantial carbon storage [1, 2]. Their intertidal location also creates interpretation challenges for Earth observation: mixed water–vegetation pixels, tidal inundation, cloud contamination and seasonality can influence satellite-derived indicators [3]. Monitoring changes in index values is therefore not equivalent to measuring changes in forest biomass, survival or ecological condition.

Sentinel-2 spectral reflectance can summarize canopy greenness through the normalized difference vegetation index (NDVI) and vegetation-associated water-sensitive reflectance through the normalized difference moisture index (NDMI). Sentinel-1 C-band synthetic aperture radar (SAR) offers cloud-independent observations, but backscatter depends on geometry, dielectric properties, acquisition configuration and tidal conditions. A dual-polarization RVI is a scattering proxy, not a direct measurement of woody structure [4–6]. Google Earth Engine (GEE) facilitates repeatable large-area satellite processing [7].

An important analytical problem is unequal annual spatial support: annual averages may change because the set of valid pixels changes. This study therefore revisits a supplied five-year Can Gio satellite export using a strictly identical pixel footprint across all years and indices. The research questions are: (i) what are the annual mean and mapped patterns of NDVI, NDMI and RVI from 2021 to 2025; (ii) what net spatial changes occur from 2021 to 2025; and (iii) how does a fixed common-support approach affect interpretation?

Mangrove ecosystems occupy narrow but environmentally important intertidal corridors, connecting terrestrial watersheds with estuaries and coastal waters. Their ecological functions include sediment trapping, shoreline stabilization, nursery habitat provision and carbon accumulation in both vegetation and waterlogged soils. The magnitude of these services is not spatially uniform: canopy architecture, species composition, geomorphology, salinity and inundation history vary across an estuarine landscape. Consequently, observations of canopy greenness alone cannot be assumed to represent the full set of ecological functions or their changes [1–3].

Can Gio, in the lower Dong Nai–Saigon estuarine region of southern Vietnam, provides a pertinent test landscape for satellite monitoring. It combines relatively continuous mangrove stands with waterways, forest margins and mixed coastal land cover. These features make interpretation difficult because reflectance and radar responses can vary within a few tens of metres across the forest–water interface. A monitoring method that averages an entire administrative or ecological region without explicitly reporting the sampled footprint can conflate changes in observation support with changes in vegetation. The study therefore defines a reference mangrove analysis domain rather than asserting that the input mask represents the entire legally designated biosphere reserve.

Optical satellite observations offer a mature approach to mapping mangrove distribution and canopy characteristics. Sentinel-2 provides visible, near-infrared and shortwave-infrared bands that support vegetation and moisture-sensitive indices. NDVI is commonly used as an indicator of spectral greenness, while NDMI reflects a contrast between near-infrared and shortwave-infrared responses associated with vegetation and canopy water-related properties. Yet these proxies have limitations: closed-canopy saturation, atmospheric residuals, shadows, seasonal changes, wet soil and water background effects can produce similar index variations for different underlying ecological processes [3, 8, 9, 11, 12].

Synthetic aperture radar provides a complementary observation modality because its active microwave signal is less constrained by cloud cover. C-band backscatter responds to canopy and surface scattering, orientation, dielectric properties and the presence of water. A dual-polarization radar vegetation index based on VV and VH intensities summarizes aspects of polarization-dependent scattering. It should not be confused with full-polarimetric measures, nor should a change in the index be equated directly with changes in branch density or above-ground biomass. In intertidal forests, tidal water beneath the canopy may alter the radar return even without any corresponding structural change [4–6, 13, 14].

Previous reviews have established the usefulness of optical, SAR and combined sensor observations for mapping mangrove extent and estimating selected structural or functional attributes [3, 6, 8, 11–16]. Studies of Sentinel-1 and Sentinel-2 integration demonstrate the potential to discriminate mangrove stages or vegetation conditions, but also highlight the need for careful preprocessing and independent validation [15, 17]. More generally, assessments of blue-carbon and canopy traits show that indirect remote-sensing indicators require calibration before conversion into biophysical quantities [18, 19]. This paper does not claim that multi-sensor integration or the constituent indices are novel inventions.

The specific analytical gap addressed here is narrower and testable: annual multi-index summaries may be compared as though they describe identical places, even when missing observations, sensor-specific masks and different composite coverage change the set of contributing pixels. Such differences can distort the apparent interannual trajectory, particularly where coastal forest margins have systematically lower valid-data coverage. The Can Gio archive provides an opportunity to compare annual NDVI, NDMI and dual-polarization RVI over one strictly shared spatial support, and to separate measured satellite-index variation from unverified ecological interpretation.

The methodological contribution is therefore a transparent downstream reanalysis of archived 2021–2025 raster products using the intersection of valid pixels across all indices and years, combined with paired pixel-level spatial differences and explicit coverage accounting. Three questions guide the study: (1) how do annual index means and spatial patterns differ on an identical reference footprint; (2) how are net 2021–2025 changes distributed among pixels rather than only reflected in domain-wide averages; and (3) which conclusions remain defensible after considering the unequal source acquisition counts, limited temporal sampling and absence of field-based validation? The expected contribution is a more cautious and reproducible screening framework, not a causal diagnosis of forest decline.

## 2. Materials and Methods

### 2.1. Study Area and Analytical Footprint

The analysis concerns a mangrove reference extent in the Can Gio estuarine landscape of southern Vietnam. The provided WorldCover 2021 mangrove reference and annual rasters use EPSG:32648 (UTM Zone 48N). The raster domain spans approximately E 690,000–720,500 m and N 1,147,700–1,180,600 m. The reference footprint is an analytical mask and must not be interpreted as the legally designated UNESCO Biosphere Reserve boundary. No independent statutory boundary was provided.

The analysis distinguishes the spatial extent of the delivered raster grid from the spatial support used for statistics. A rectangular raster boundary contains many non-mangrove or invalid pixels; it is not the denominator for the reported mean. The fixed reference mask is based on the supplied WorldCover 2021 product, which describes a reference land-cover class at one time. Using this fixed mask improves like-for-like observation but does not establish that all pixels remained mangrove throughout the five-year period. A formal reserve boundary would be needed for reserve-wide area statements.

All area estimates in the reanalysis are derived from the delivered projected pixel grid. Each pixel is 20 m × 20 m, or 400 m² (0.04 ha), so the 818,487 common valid pixels correspond to 32,739.48 ha. This number is the analyzed intersection area, not an independently validated estimate of

mangrove extent. The coordinate system EPSG:32648 allows area calculations from planar pixel dimensions at the reported map scale, subject to the usual projection and classification limitations.

### 2.2. Input Datasets and Index Definitions

The supplied archive contains 32 files: annual NDVI, NDMI and RVI GeoTIFFs for 2021–2025; annual observation-count and validity-mask rasters; fixed-coverage masks; a WorldCover 2021 reference raster; a scene manifest; annual summary statistics; and three exported 2021–2025 change rasters. The analysis rasters are 1,525 × 1,645 pixels, EPSG:32648, with a 20 × 20 m pixel grid. Thus, the delivered analysis grid is 20 m, not the 10 m grid asserted in the older draft.

The manuscript index definitions are NDVI = (NIR − Red)/(NIR + Red), NDMI = (NIR − SWIR1)/(NIR + SWIR1), and dual-polarization RVI = 4VH/(VV + VH), with VV and VH radar intensities in linear power units. The archive does not include the complete GEE script or all per-scene preprocessing settings. Consequently, the original image filtering, speckle treatment, orbit selection and order of index/composite operations cannot be independently reconstructed from this archive. We do not claim these upstream steps have been verified.

For the optical indices, the normalized differences are dimensionless ratios. NDVI = (NIR − Red)/(NIR + Red) and NDMI = (NIR − SWIR1)/(NIR + SWIR1). For the radar product, RVI = 4VH/(VV + VH) is the formulation reported in the study documentation; VV and VH must be expressed in linear power rather than logarithmic decibels. This definition and the upstream implementation should be checked against the executable source before a fully reproducible processing claim can be made. The downstream work in this manuscript uses the exported index values as provided and does not reconstruct missing original scene-level operations.

Optical reflectance, radar intensity and the derived indices have different measurement physics. The indices are therefore compared as parallel time series, not combined into an uncalibrated composite "forest health score." No universal ecological thresholds are imposed on their values. Water exclusion and land-cover reference masking may reduce obvious non-forest contamination, but the source archive alone cannot demonstrate that tidal stage, edge mixing and residual atmospheric effects were uniformly removed in every annual composite.

### 2.3. Common-Support Statistics and Change Maps

The third band of anGio_FixedCoverageMasks_2021_2025.tif (Common_Fixed_2021_2025) was selected where its value equals 1. This mask was intersected with finite-value masks from every annual NDVI, NDMI and RVI raster. The resulting identical support contains 818,487 pixels (32,739.48 ha at 400 m² per pixel). Every annual mean was recomputed as the arithmetic average of values on these exact pixels. No inference about independently sampled forest plots or statistical significance was made.

For each index, the 2025–2021 difference was calculated pixel by pixel on the same support. Maps use index-specific fixed display ranges for annual panels. Change maps use symmetric display limits based on the 95th percentile of the absolute change solely for visualization. Such visualization limits are not ecological degradation thresholds.

Let M denote the binary common-support mask and I(k,t,p) the value of index k in year t at pixel p. The annual mean is $\mu(k,t) = [\Sigma(p \in M)\, I(k,t,p)]/N$, where N = 818,487. For paired change, $\Delta I(k,p) = I(k,2025,p) - I(k,2021,p)$. The domain mean of paired differences equals the difference of annual means because the exact same pixels enter both expressions. The pixel distribution is summarized by its median, first and third quartiles, and the fractions with positive and negative differences. A zero difference is neither assigned to the positive nor negative class.

The fixed mask is constructed as the logical intersection of the supplied common-coverage band and finite-value masks of all fifteen annual index rasters. This is intentionally conservative: if a pixel is invalid in any year or any index, it is excluded from all annual means. The procedure avoids shifting sample composition but reduces spatial coverage and may favor locations that are consistently observable. Results must thus be described as conditional on the common-support domain rather than representative of all coastal vegetation.

The annual maps are displayed using fixed index-specific scales, so apparent differences in map color do not arise from re-stretching each year separately. For change maps, a symmetric range around zero is set using the 95th percentile of absolute paired differences to preserve the visual distinction between positive and negative values. Values beyond the limits are visually saturated but remain included in numerical statistics. This display operation is not a significance test and does not establish biologically meaningful degradation thresholds.

### 2.4. Data Provenance and Limits of Reproducibility

The CSV manifest documents exported scene metadata, and the annual statistics file records scene counts and valid-area summaries. These products enable independent downstream raster calculations, but full end-to-end GEE reproducibility still requires the original executable script, processing parameters and source boundary definition. No field validation, tidal-stage measurements, independent biomass observations or causal attribution dataset was supplied.

The scene-count and annual valid-area values are treated as provenance information reported by the exported CSV. They are not recalculated from source image collections. Because the original GEE script is unavailable, no claim is made that the precise optical cloud screening, SAR orbit composition or annual compositing algorithm has been independently audited. This separation of upstream uncertainty from verified raster arithmetic is essential to the interpretation of the results.

### 2.5. Post-Export Audit and Cross-Sensor Comparison

A reproducible post-export audit read the original GeoTIFF files on their shared EPSG:32648, 20-m grid, calculated the strict intersection of the five-year optical and radar masks, and recomputed annual means and 2025-minus-2021 differences on this population. Separate annual and paired-year footprints were retained as comparison populations; the pairwise footprint was defined by valid values in both endpoint years. We report the reference-to-common retention fraction, direction of pixel changes, pairwise Pearson correlations and concordant versus discordant signs. All metrics are descriptive and are not used as significance tests.

## 3. Results

### 3.1. Image Availability and Fixed-Support Annual Means

**Table 1:** Counts and reported common valid area from the supplied annual-statistics CSV; these original summary areas are distinct from the strict intersection mask used below.

| Year | S1 scenes | S2 scenes | Reported common valid area (ha) |
|---|---|---|---|
| 2021 | 120 | 95 | 35,157.3 |
| 2022 | 81 | 85 | 35,168.5 |
| 2023 | 64 | 96 | 35,168.5 |
| 2024 | 58 | 96 | 32,736.4 |
| 2025 | 89 | 95 | 35,157.6 |

**Table 2:** Independently recalculated means on the identical 818,487-pixel footprint for every index and year.

| Year | NDVI mean | NDMI mean | RVI mean | Common pixels |
|---|---|---|---|---|
| 2021 | 0.8034 | 0.4994 | 0.7952 | 818,487 |
| 2022 | 0.8234 | 0.5207 | 0.7932 | 818,487 |
| 2023 | 0.8095 | 0.5099 | 0.7916 | 818,487 |
| 2024 | 0.8147 | 0.5091 | 0.7981 | 818,487 |
| 2025 | 0.8070 | 0.5021 | 0.7854 | 818,487 |

NDVI and NDMI were highest in 2022, while RVI was highest in 2024 and lowest in 2025. The 2024 RVI maximum persists even when restricting all years to the same pixel support; it cannot therefore be attributed solely to the different valid-pixel count in the unharmonized annual means. However, acquisition-season and tidal confounding remain unresolved.

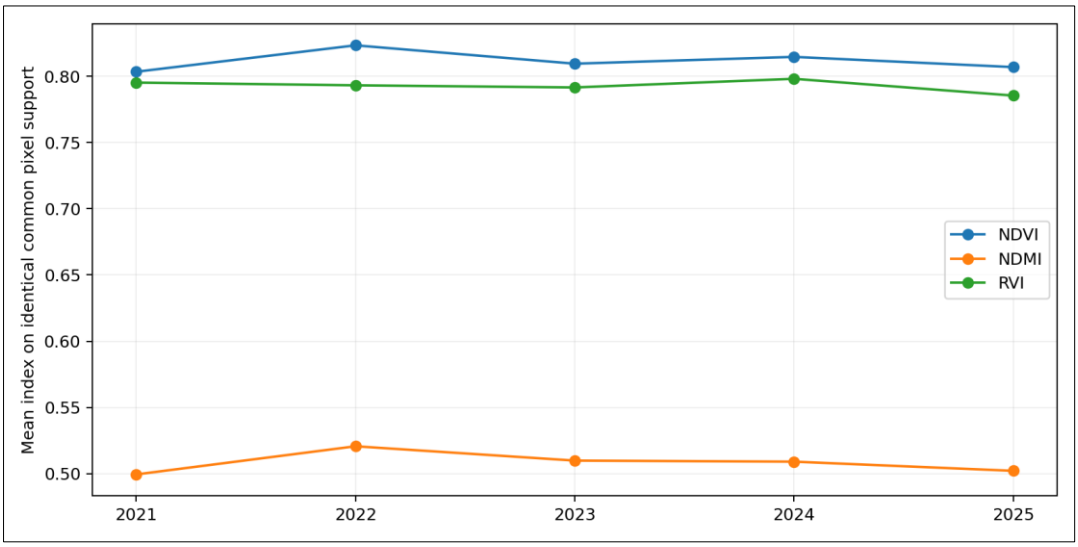


**Fig 1:** Annual index trajectories on identical common spatial support.

The five annual means are not monotonic. NDVI rose from 0.8034 in 2021 to 0.8234 in 2022, fell to 0.8095 in 2023, partially recovered to 0.8147 in 2024 and ended at 0.8070 in 2025. NDMI followed a broadly similar sequence, with its maximum in 2022 (0.5207) and 2025 value of 0.5021. In contrast, RVI decreased from 0.7952 in 2021 to 0.7916 in 2023, increased to 0.7981 in 2024, and reached 0.7854 in 2025. The 2024 RVI maximum is particularly important because the underlying acquisition counts and original valid area differ from other years.

Comparing annual averages alone would conceal the distinct acquisition conditions of the optical and radar datasets. The scene manifest reports 120 Sentinel-1 scenes in 2021 but only 58 in 2024, while the number of Sentinel-2 scenes is comparatively stable across the study period. These counts do not measure per-pixel observation frequency or tidal balance, but they provide a transparent warning against attributing every difference to canopy processes. The common mask solves one comparability problem—changing pixel location—but not the temporal sampling problem.

### 3.2. Annual Spatial Distributions

Figures 2–4 retain the full available spatial footprint of the original annual maps. The five-year common-valid-pixel intersection was used separately for the comparable numerical summaries; the broader annual displays must not be interpreted as maps of that intersection.

The persistent channels and narrow coastal margins visible in the maps also illustrate a resolution-related constraint. At 20 m, a pixel can contain canopy, water and exposed substrate, and the relative mixture may change with tide and geolocation. This is particularly relevant to the apparent spatial heterogeneity near boundaries. Therefore, pixelwise changes are retained as continuous values rather than immediately converted into forest-loss categories.

### 3.3. Net Changes, 2021–2025

From 2021 to 2025, the common-support mean NDVI increased by +0.0035, NDMI increased by +0.0027, and RVI declined by −0.0098 (index units; values rounded). These small domain-average differences coexist with spatially heterogeneous positive and negative pixel-level changes. The maps do not establish ecological improvement or damage without independent validation.

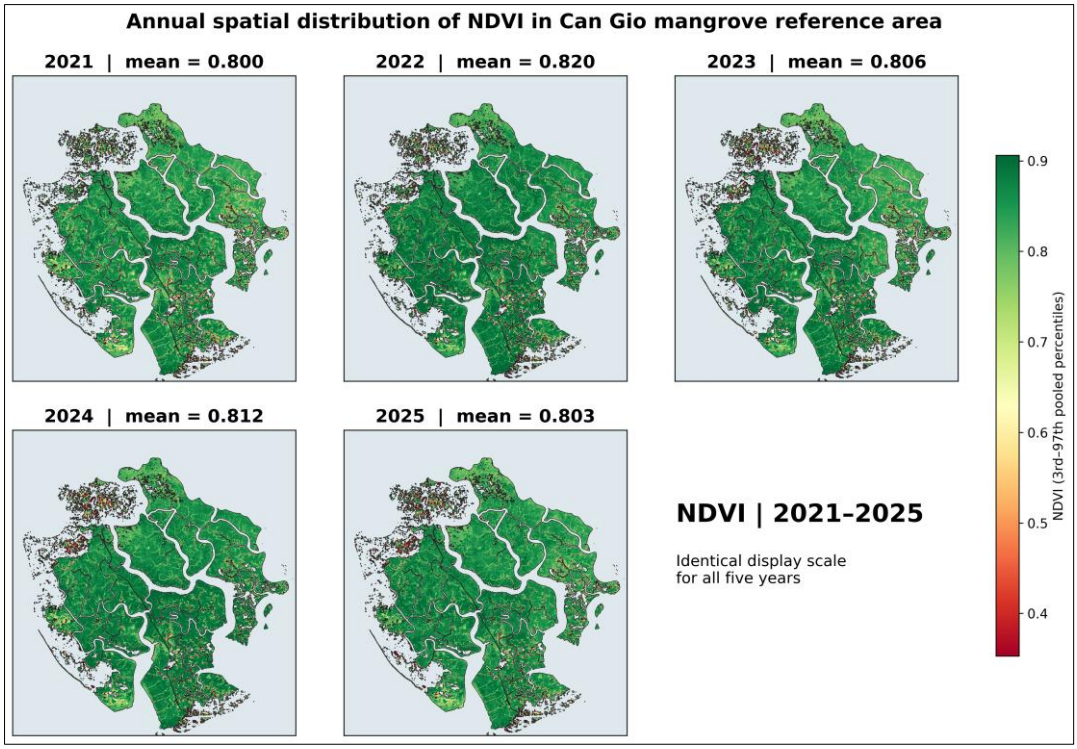


**Fig 2:** Annual NDVI raster maps (2021–2025), showing the complete annual mapped extent. Displayed map coverage is not the five-year intersection mask used for comparative statistics.

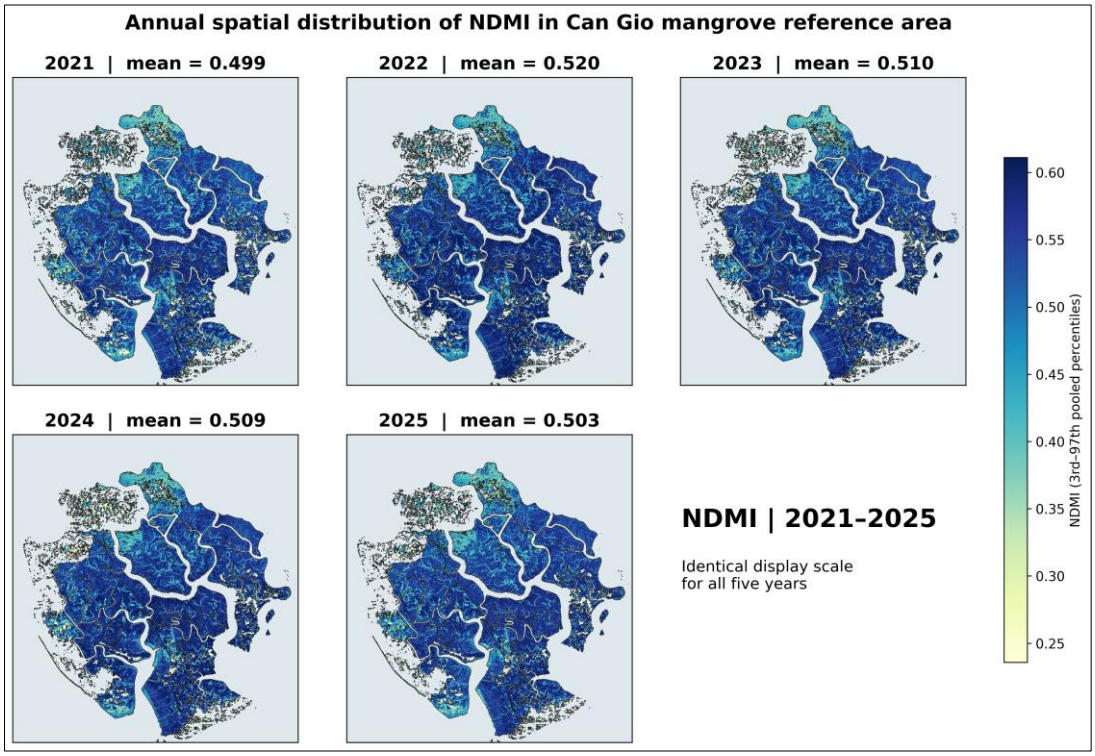


**Fig 3:** Annual NDMI raster maps (2021–2025), showing the complete annual mapped extent. Displayed map coverage is not the five-year intersection mask used for comparative statistics.

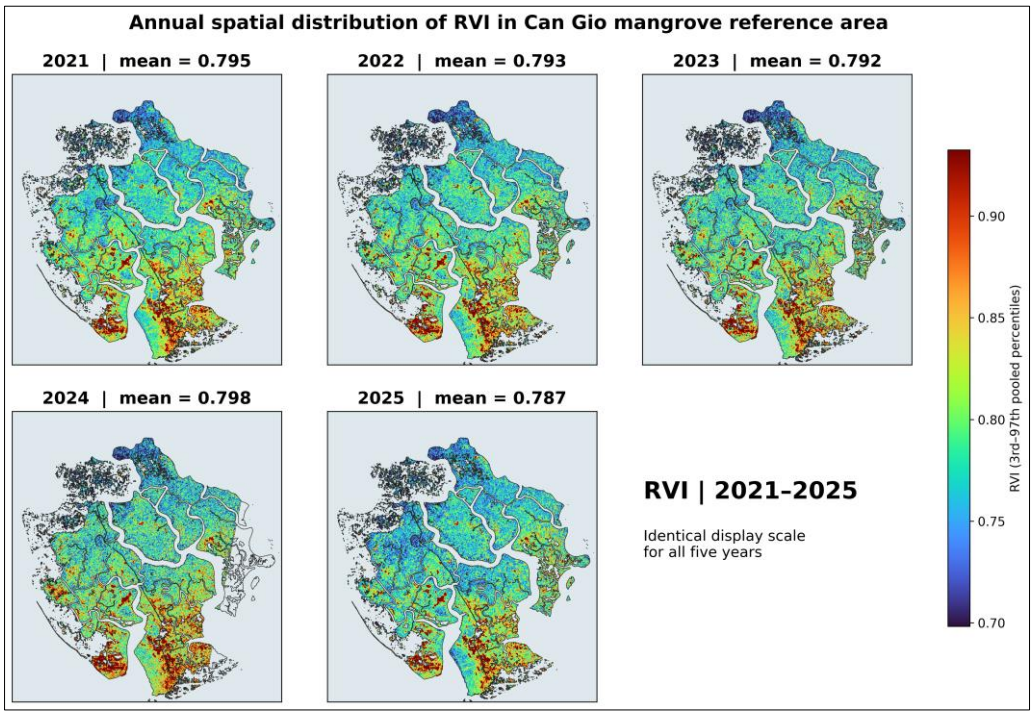


**Fig 4:** Annual dual-polarization RVI raster maps (2021–2025), showing annual valid coverage, including reduced coverage in 2024. Statistical comparisons use the common-valid-pixel mask.

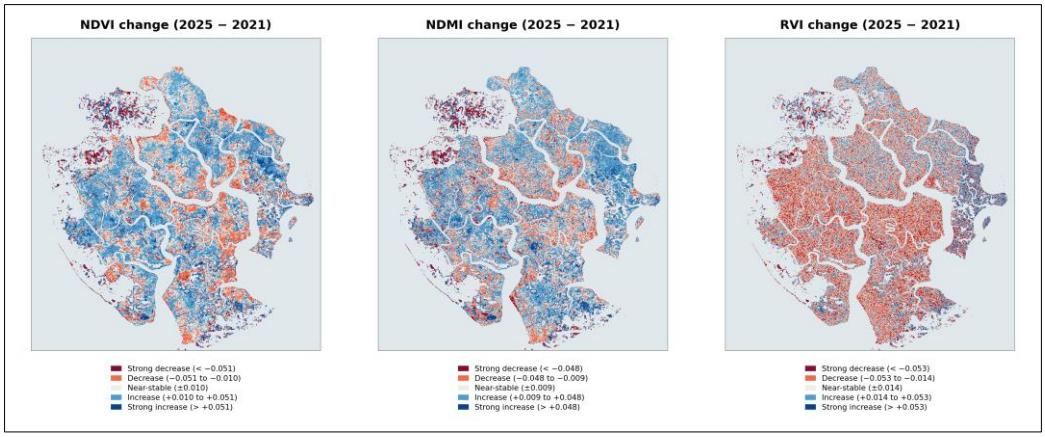


**Fig 5:** Spatial differences in NDVI, NDMI and RVI (2025 minus 2021), recomputed directly from paired annual GeoTIFFs over their valid paired-year footprints (879,187 pixels for NDVI and NDMI; 879,726 for RVI). Five display classes use index-specific thresholds; grey denotes unavailable paired-year data. These display footprints are broader than the strict five-year, three-index common mask (818,487 pixels) used for annual means and Table 3.

On the common support, the 2021–2025 differences in mean indices are approximately +0.00352 for NDVI, +0.00271 for NDMI and −0.00980 for RVI. Expressed relative to the 2021 mean, these correspond to approximately +0.44%, +0.54% and −1.23%, respectively. These percentages are changes in index means, not percentage changes in biomass, canopy area or forest health. The spatial difference map illustrates that positive and negative changes can coexist even when the overall mean shift is small.

Paired maps and summary quantiles are more informative than a single domain-wide percentage because opposing changes may cancel. The sign of a pixel-level difference also does not identify the mechanism behind it: a decrease in NDMI might reflect differences in leaf and background water sensitivity, while a decrease in RVI might reflect altered scattering geometry or inundation. Consequently, no hectares of "degraded mangrove" are reported from unvalidated index thresholds.

### 3.4. Spatial-Change Distribution

Table 3 reports the sign and interquartile distribution of paired changes on the same 818,487-pixel population. The fraction of positive and negative pixels provides a reproducible descriptive account of spatial heterogeneity. However, neighboring pixels are spatially autocorrelated, and these fractions are not independent Bernoulli trials. We therefore avoid treating the very large number of pixels as an equally large number of independent ecological observations or using it to manufacture extremely small p-values.

**Table 3:** Distribution of paired 2025–2021 differences. Percentages refer only to the common valid footprint and are not estimates of forest gain or loss.

| Index | Median Δ | Q1 Δ | Q3 Δ | Positive pixels | Negative pixels |
|---|---|---|---|---|---|
| NDVI | +0.0085 | -0.0076 | +0.0251 | 64.2% | 35.8% |
| NDMI | +0.0074 | -0.0078 | +0.0236 | 63.2% | 36.8% |
| RVI | -0.0095 | -0.0327 | +0.0137 | 39.1% | 60.9% |

### 3.5. Quantitative Audit of Spatial Support and Multi-Sensor Agreement

Reanalysis of the supplied 20-m GeoTIFF products identified 879,726 pixels in the WorldCover-derived reference footprint and 818,487 pixels in the strict five-year joint support (93.04% retained; 6.96% excluded). The reference footprint therefore covers 35,189.04 ha and the strict support 32,739.48 ha. These are raster-cell areas, not independently validated mangrove extents. All following change statistics use exactly the same 818,487 pixels.

Between 2021 and 2025, strict-support mean changes were +0.003524 for NDVI, +0.002710 for NDMI and −0.009802 for RVI. Positive changes occurred in 64.15%, 63.15% and 39.11% of pixels, respectively. These are descriptive changes in annual index composites, not estimates of forest growth, loss or canopy degradation.

Pixel-level Pearson correlations between 2025–2021 changes were 0.8342 (NDVI–NDMI), 0.2726 (NDVI–RVI) and 0.2553 (NDMI–RVI). Same-sign changes represented 74.00%, 48.62% and 49.21% of pixels, respectively; the complementary opposite-sign fractions were 26.00%, 51.37% and 50.79%. These spatial associations indicate that optical indices agree more closely with one another than with the radar index, but spatial autocorrelation and acquisition differences preclude treating pixel counts as independent inferential replicates.

The supplied export code was identified as Can gio V2.2 (2021–2025), not the earlier four-year V2 code. It computes per-scene RVI after conversion from dB to linear power, then annual median composites; it exports annual optical/radar masks and five-year fixed masks. This establishes a plausible processing specification, but code–raster identity still requires a rerun or provenance check. The source script uses scale and CRS without a fixed affine transform in the export call, which should be locked for future production runs.

## 4. Discussion

### 4.1. Divergent Optical and Radar Trajectories

The analysis indicates a modest net increase in optical indices from 2021 to 2025 alongside a modest decline in RVI. This divergence is consistent with the fact that optical and C-band microwave observations respond to different physical properties, but it does not demonstrate a specific process of woody-branch dieback. Radar scattering can vary with surface water, tidal stage, geometry, dielectric properties and processing choices [4–6]. Equally, high NDVI or NDMI does not independently verify ecological health or foliar water content.

The optical maxima in 2022 are consistent with a period of relatively high spectral greenness and moisture-sensitive response in the delivered composites. They cannot be interpreted as an ecological optimum without field observations and careful seasonal controls. Reviews of mangrove indices emphasize that optical vegetation metrics can be affected by canopy density, background reflectance, atmospheric contamination and the water environment [3, 8, 11]. The five-year optical record therefore supports a descriptive comparison, not a diagnosis of canopy vigor or physiological stress.

The radar series differs: the RVI peak occurs in 2024 and its minimum in 2025. Dual-polarization indices can be useful for characterizing scattering changes, but their physical meaning is not identical to full-polarimetric decomposition or field-measured structure [4, 5, 13, 17]. In mangroves, inundated trunks and water surfaces may contribute to scattering responses. It would therefore be unsound to interpret the 2025 decline as direct evidence of branch mortality, stem loss or erosion without tidal matching and ground verification.

The differences between index trajectories are themselves useful because they identify places and times at which a single-sensor explanation may be incomplete. Multisensor literature supports combining complementary observations to improve monitoring robustness [6, 15–17]. Here, however, the indices are not fused into a calibrated model and no independent classification accuracy is available. The principal empirical contribution is an auditable comparison on a common pixel support rather than a new structural retrieval algorithm.

### 4.2. Why the Common Spatial Support Matters

The supplied annual statistics report a reduced common valid area in 2024. A simple comparison of unharmonized annual means may confound spatial sampling with temporal change. Here, all 15 annual index rasters were evaluated over exactly 818,487 identical pixels, making the reported arithmetic means spatially comparable. Nevertheless, a common mask does not eliminate differences in acquisition dates, scene counts, observation geometry, tidal conditions or seasonal composition. In particular, only 58 Sentinel-1 scenes were listed for 2024 compared with 120 for 2021.

A fixed mask is a simple but consequential design choice. When each annual mean uses a different set of pixels, apparent change can arise even if every retained location were stable. The reported 2024 valid-area reduction in the source statistics makes this concern concrete. Recalculating all indices on one intersection support ensures that year-to-year differences are not explained by changing membership of the sample pixels. This procedure is particularly appropriate for retrospective comparisons in coastal landscapes with persistent cloud and water-related missingness.

The solution also has a cost. The intersection selects consistently observable pixels and discards all locations that were invalid in any annual layer. The retained area is therefore smaller than most year-specific valid areas and may underrepresent challenging tidal edges. The mean trajectories describe this restricted population, not the full mangrove extent. An ideal extension would compare complete-case,

pairwise-intersection and annual-support estimates, quantify excluded-pixel geography and investigate whether the exclusion is associated with water proximity or forest structure.

Coverage harmonization should also be distinguished from temporal harmonization. The original composites may differ in seasonal balance, orbit geometry, rain conditions and water levels even after identical pixels are selected. Annual scene counts cannot substitute for per-pixel acquisition dates and tide records. Future work should stratify SAR by orbit and tidal stage, and optical scenes by season and observation density, to test whether the observed index differences persist under matched conditions.

### 4.3. Practical Implications and Validation Priorities

The spatial difference layers can prioritize field inspections where optical and radar proxies show unusually large or opposing changes. Such screening should be followed by independent vegetation plots, repeat field photography, shoreline-change mapping, salinity and inundation measurements, and tide-stratified SAR analysis before management decisions or degradation labels are assigned. Comparisons with independent reference maps and robust sensitivity analysis would strengthen interpretation.

The monitoring implications differ depending on the intended decision. For broad screening, the most useful outputs may be the spatial continuity of anomalies, their persistence across years and their concurrence among independent sensors. For formal estimation of mangrove area, biomass or ecological damage, however, the relevant outputs must be linked to validated reference classes and uncertainty intervals. The current data meet the former descriptive purpose but not the latter inferential purpose. This distinction matters because numerical precision in a raster index should not be mistaken for ecological accuracy.

An additional methodological issue is the spatial scale at which changes are summarized. A whole-domain average can remain nearly unchanged when opposing local shifts cancel, whereas an individual 20-m pixel may be unusually sensitive to mixed land cover or georegistration. Future studies should therefore report changes at several aggregation scales, for example small neighborhood blocks and management sectors, and evaluate whether apparent hotspots remain stable as the analysis unit changes. Such multiscale checks would help distinguish isolated pixel noise from coherent spatial signals, although field evidence would still be required to label a biological impact.

Comparison with regional and global literature should be framed around methodological consistency rather than direct numerical equivalence of index values. Published studies differ in their forest masks, sensors, compositing seasons, radar incidence angles and definitions of ecological condition. It would be inappropriate to infer that an RVI value observed here corresponds to the same canopy structure in a different mangrove species assemblage or tidal setting. More useful comparisons concern whether studies control acquisition conditions, report spatial support and validate inferred structural changes with independent observations.

For local managers, the practical output is a prioritization layer rather than a definitive forest-condition map. Locations with large paired changes or disagreement among optical and radar proxies can be selected for site visits, repeated photographs and vegetation measurements. Independent shoreline mapping would be necessary before attributing margin signals to erosion, while salinity, rainfall and tidal observations would be needed to test environmental mechanisms. This targeted approach is more defensible than imposing generic thresholds and labeling areas as degraded solely from an index.

An operational monitoring workflow could combine repeated Sentinel composites with a permanent set of field plots and explicit uncertainty tracking. At each update, it would report the spatial support, observation counts, per-pixel missingness and the stability of index patterns under alternative masks. *In situ* tree survival, basal area, canopy cover and porewater salinity would provide the external observations required to relate remote-sensing variability to ecological outcomes. The present results can guide where those additional observations may be most informative.

This restrained interpretation is consistent with broader literature on mangrove mapping, carbon and canopy-trait retrievals, where sensor measurements are valuable but biophysical estimates depend on reference observations, model transferability and uncertainty reporting [12, 16, 18–20]. The Can Gio analysis should therefore be positioned as a reproducible descriptive screening study with a clear pathway to subsequent ecological validation.

### 4.4. Limitations

The five-year series contains only five annual observations; it cannot establish a statistically robust long-term trend or causal mechanism. The archive lacks full executable upstream GEE code and field validation. The WorldCover 2021 mask is not a verified annual mangrove-persistence layer, and the analysis domain is not the statutory reserve polygon. The index distributions may reflect mixed pixels and tidal hydrology. No claims about mortality, carbon-stock change, erosion caused by navigation or climate-driven salinity stress are supported directly by these inputs.

Several limitations affect the strength of inference. First, five annual composites provide only five time points, and no trend significance or climate attribution is claimed. Second, the supplied reference class is from 2021 and cannot verify mangrove persistence to 2025. Third, the original processing script and detailed per-scene choices were not supplied, so only downstream raster calculations are independently reproducible from the archive. Fourth, there are no independent field measurements, tide-matched radar composites or spatially explicit validation samples. Fifth, adjacent pixels are not independent observations, and continuous index differences should not be mistaken for mapped forest-loss events.

These limitations do not invalidate the measured raster summaries, but they define the claims that the manuscript can support. Future analyses should release executable processing code and parameter settings, establish a documented boundary and independent mangrove reference, evaluate alternate compositing periods, quantify uncertainty with spatially aware sampling and validate proposed ecological classes in the field. Such work would convert the present screening maps into stronger evidence for management decisions.

The additional comparison shows that common spatial support excludes 6.96% of the reference footprint, a potential source of selection bias if excluded pixels cluster near channels or forest margins. This supports reporting retained area and exclusion maps rather than treating the intersection as inherently unbiased. Weak optical–radar change correlations further justify a multi-sensor description, but do not independently establish ecological change. A matched-season, orbit-aware rerun is necessary before attributing the 2024 RVI maximum or 2025 decline to canopy processes.

## 5. Conclusion

This study evaluated mangrove canopy-related satellite signals in Can Gio, Vietnam, using annual Sentinel-2 NDVI and NDMI and Sentinel-1 dual-polarization RVI rasters for 2021–2025. By restricting all comparisons to the same 818,487 valid pixels (32,739.48 ha at 20-m pixel spacing), the analysis reduced the spatial-support bias that can arise when annual summaries use different valid-data footprints. The resulting common-support series showed the highest mean NDVI (0.8234) and NDMI (0.5207) in 2022, whereas mean RVI reached its lowest value (0.7854) in 2025. Between 2021 and 2025, the corresponding mean changes were approximately +0.0035 for NDVI, +0.0027 for NDMI and −0.0098 for RVI. These small net changes and the contrasting annual trajectories show why optical and radar indicators should be evaluated together rather than treated as interchangeable measures of forest condition.

Spatial difference maps further reveal heterogeneous patterns within the fixed reference footprint, offering a reproducible basis for identifying locations where follow-up observations may be most informative. However, index variation alone does not establish canopy mortality, biomass decline, shoreline erosion or specific climatic drivers. In particular, dual-polarization RVI can respond to moisture, inundation and acquisition geometry as well as vegetation scattering. The fixed 2021 mangrove reference, lack of field validation and incomplete upstream GEE processing record limit ecological attribution. The main contribution is therefore a transparent, spatially consistent multi-sensor assessment framework, rather than a validated degradation map. Future work should pair tide-aware radar processing and fully documented GEE scripts with independent field observations, mangrove reference updates and spatially explicit uncertainty analysis before using these products for operational ecological classification.

## References


1. Alongi DM. Mangrove forests: resilience, friability and response to global climate change. Ambio. 2008;37:540–548. doi:10.1579/0044-7447-37.7.540.
2. Donato DC, Kauffman JB, Murdiyarso D, *et al*. Mangroves among the most carbon-rich forests in the tropics. Nat Geosci. 2011;4:293–297. doi:10.1038/ngeo1123.
3. Kuenzer C, Bluemel A, Gebhardt S, Quoc TV, Dech S. Remote sensing of mangrove ecosystems: a review. Remote Sens. 2011;3:878–928. doi:10.3390/rs3050878.
4. Simard M, Rivera-Monroy VH, Mancera-Pineda JE, *et al*. A systematic method for 3D mapping of mangrove forests using Shuttle Radar Topography Mission elevation data. Remote Sens Environ. 2006;102:310–331. doi:10.1016/j.rse.2006.02.020.
5. Kim Y, Jackson T, Bindlish R, Lee H, Hong S. Radar vegetation index for polarimetric SAR observations. IEEE Trans Geosci Remote Sens. 2012;50:1084–1094. doi:10.1109/TGRS.2011.2164553.
6. Pham TD, Yokoya N, Bui DT, Yoshino K, Friess DA. Remote sensing approaches for monitoring mangrove species, structure, and biomass: opportunities and challenges. Remote Sens. 2019;11:230. doi:10.3390/rs11030230.
7. Gorelick N, Hancher M, Dixon M, *et al*. Google Earth Engine: planetary-scale geospatial analysis for everyone. Remote Sens Environ. 2017;202:18–27. doi:10.1016/j.rse.2017.06.031.
8. Tran TV, Reef R, Zhu X. A review of spectral indices for mangrove remote sensing. Remote Sens. 2022;14:4868. doi:10.3390/rs14194868.
9. Xu H. Modification of normalised difference water index (NDWI) to enhance open water features in remotely sensed imagery. Int J Remote Sens. 2006;27:3025–3033. doi:10.1080/01431160600589179.
10. Nguyen AB, Hauser LT, Salinero-Delgado M, *et al*. Monitoring mangrove traits through optical Earth observation: towards spatio-temporal scalability using cloud-based Sentinel-2 continuous time series. ISPRS J Photogramm Remote Sens. 2024;214:135–152. doi:10.1016/j.isprsjprs.2024.06.007.
11. Maurya K, Mahajan S, Chaube N. Remote sensing techniques: mapping and monitoring of mangrove ecosystem—a review. Complex Intell Syst. 2021;7:2797–2818. doi:10.1007/s40747-021-00457-z.
12. Thakur S, Mondal I, Ghosh PB, Das P, De TK, *et al*. A review of the application of multispectral remote sensing in the study of mangrove ecosystems with special emphasis on image processing techniques. Spat Inf Res. 2020;28:39–51. doi:10.1007/s41324-019-00268-y.
13. Giri C. Recent advancement in mangrove forests mapping and monitoring of the world using Earth observation satellite data. Remote Sens. 2021;13:563. doi:10.3390/rs13040563.
14. Lu Y, Wang L. The current status, potential and challenges of remote sensing for large-scale mangrove studies. Int J Remote Sens. 2022;43:6824–6855. doi:10.1080/01431161.2022.2145584.
15. Upakankaew K, Ninsawat S, Virdis SGP, Sasaki N. Discrimination of mangrove stages using multitemporal Sentinel-1 C-band backscatter and Sentinel-2 data—a case study in Samut Songkhram Province, Thailand. Forests. 2022;13:1433. doi:10.3390/f13091433.
16. Nguyen AB, Hauser LT, Hoa PV, *et al*. Quantifying mangrove leaf area index from Sentinel-2 imagery using hybrid models and active learning. Int J Remote Sens. 2022;43:5636–5657. doi:10.1080/01431161.2021.2024912.
17. Metternicht GI, Zinck JA. Remote sensing of soil salinity: potentials and constraints. Remote Sens Environ. 2003;85:1–20. doi:10.1016/S0034-4257(02)00188-8.

18. Technological opportunities for measuring and monitoring blue carbon initiatives in mangrove ecosystems. Remote Sens Appl Soc Environ. 2021;24:100612. doi:10.1016/j.rsase.2021.100612.
19. Remote sensing-based assessment of mangrove ecosystems in the Gulf Cooperation Council countries: a systematic review. Front Mar Sci. 2023. doi:10.3389/fmars.2023.1241928.
20. Giri C, Ochieng E, Tieszen LL, *et al*. Status and distribution of mangrove forests of the world using earth observation satellite data. Glob Ecol Biogeogr. 2011;20:154–159. doi:10.1111/j.1466-8238.2010.00584.x.

**How to Cite This Article**

Hoang TT, Ngo TMT, Le TLT. Multi-sensor assessment of mangrove canopy dynamics in Can Gio, Vietnam, using Sentinel-1 and Sentinel-2. International Journal of Multidisciplinary Comprehensive Research. 2026;5(6):14–23. doi:10.54660/IJMCR.2026.5.6.14-23.

**Creative Commons (CC) License**

This is an open access journal, and articles are distributed under the terms of the Creative Commons Attribution-NonCommercial-ShareAlike 4.0 International (CC BY-NC-SA 4.0) License, which allows others to remix, tweak, and build upon the work non-commercially, as long as appropriate credit is given and the new creations are licensed under the identical terms.